Photoelectron spectroscopy of phosphorus hydride anions

Kent M. Ervin[a)]
Department of Chemistry and Chemical Physics Program, University of Nevada, Reno, Reno, Nevada 89557

W. Carl Lineberger
JILA, University of Colorado and National Institute of Standards and Technology, and Department of Chemistry and Biochemistry, University of Colorado, Boulder, Colorado 80309-0440

(Received 8 December 2004; accepted 4 February 2005; published online 13 May 2005)

Negative-ion photoelectron spectroscopy is applied to the PH^-, PH_2^-, P_2H^-, $P_2H_2^-$, and $P_2H_3^-$ molecular anions. Franck–Condon simulations of the photoelectron spectra are used to analyze the spectra and to identify various $P_2H_n^-$ species. The simulations employ density-functional theory calculations of molecular geometries and vibrational frequencies and normal modes, and coupled-cluster theory calculations of electron affinities. The following electron affinities are obtained: $EA_0(PH)=1.027\pm0.006$ eV, $EA_0(PH_2)=1.263\pm0.006$ eV, and $EA_0(P_2H)=1.514\pm0.010$ eV. A band is identified as a mixture of *trans*-$HPPH^-$ and *cis*-$HPPH^-$. Although the *trans* and *cis* bands cannot be definitively assigned from experimental information, using theory as a guide we obtain EA_0(*trans*-HPPH)$=1.00\pm0.01$ eV and EA_0(*cis*-HPPH)$=1.03\pm0.01$ eV. A weak feature tentatively assigned to $P_2H_3^-$ has a vertical detachment energy of 1.74 eV. The derived gas-phase acidity of phosphine is $\Delta_{acid}G_{298}(PH_3)\leqslant 1509.7\pm2.1$ kJ mol^{-1}. © *2005 American Institute of Physics*. [DOI: 10.1063/1.1881153]

I. INTRODUCTION

Phosphorus hydride compounds and radicals are of interest in planetary atmospheres and other astrophysical environments.[1,2] They are also important because of the role of organophosphorus compounds in catalysis of radical recombination reactions involved in combustion[3,4] and because of the use of phosphine in chemical-vapor deposition of phosphide semiconductors.[5–7] Fundamentally, accurate descriptions of multiply bonded compounds of third-row elements by theoretical methods[4,8–15] is a challenging problem. Whereas neutral phosphanes have been studied extensively,[16] their radical and anionic fragments are less well characterized. In this work, we apply negative-ion photoelectron spectroscopy to a series of phosphorus hydride anions, PH^-, PH_2^-, P_2H^-, $P_2H_2^-$, and $P_2H_3^-$. We identify the transitions between electronic and vibrational levels of the anions and the corresponding neutrals and we report electron affinities and other molecular constants. The photoelectron spectra of PH^- and PH_2^- have been reported previously[17–19] but are obtained here with higher resolution allowing rotational contours to be examined and more precise electron affinities to be obtained. The photoelectron spectra of the diphosphorus hydride anions, $P_2H_n^-$ ($n=1-3$), are reported for the first time.

II. METHODS

Negative-ion photoelectron spectroscopy is performed by crossing a mass-selected ion beam with a fixed-frequency laser. The kinetic energies of photodetached electrons are measured with an electrostatic energy analyzer to obtain the photoelectron spectrum of transitions between initial states of the anion and final states of the corresponding neutral species. Electron binding energies (*e*BEs) of observed transitions are given by the photon energy minus the measured electron kinetic energy (*e*KE). The experimental techniques and data analysis procedures have been described in detail in previous reports.[20–23]

Phosphorus hydride anions are produced by injecting phosphine (PH_3) into a flowing afterglow ion source downstream of a microwave discharge, using helium buffer gas at a total pressure of 0.3–0.5 Torr. Phosphine is a highly toxic gas that requires special handling procedures. The PH_3 lecture bottle, regulator, and gas handling system were enclosed in a vented cabinet. The major anion formed is PH_2^- (typically 60 pA), with smaller amounts of PH^- (5 pA) and P^- (8 pA). Diphosphorus hydride species ($P_2H_n^-$, 10–20 pA) are presumably produced by secondary-ion–molecule reactions of PH_n^- species with PH_3. Ions of a particular mass are selected by passage through a Wien velocity filter. The mass resolution is sufficient to separate PH_n^- ions completely, but partial mass overlap occurs among various $P_2H_n^-$ species.

This work employs the 351.1-nm (3.531 eV) or 363.8-nm (3.408 eV) lines of an argon-ion laser, amplified to 30–40 W in a power build-up cavity, to induce photodetachment.[22] The resolution of the hemispherical electrostatic energy analyzer is enhanced by imaging the output photoelectrons onto a position-sensitive anode detector.[20] The resolution of the kinetic-energy analyzer is 5–8 meV over the entire energy range. The electron kinetic-energy scale is calibrated from the photoelectron spectrum of atomic phosphorus anions, described in detail below. The experimental uncertainty in the absolute electron kinetic energy of

a)Electronic mail: ervin@chem.unr.edu

TABLE I. Electron affinities (eV).

Species	Theory[a]	Expt.	Ref.
P	0.613 (0.734)	0.7465±0.0003	33 and 34
PH	0.922 (1.026)	1.027±0.006	This work
		1.028±0.010	18
		1.00±0.06	17
PH_2	1.201 (1.271)	1.263±0.006	This work
		1.271±0.010	18
		1.25±0.03	19
P_2	0.562	0.589±0.025	56
		0.63±0.05	57
P_2H	1.462	1.514±0.010	This work
trans-HPPH[b]	1.008	1.00±0.01	This work
cis-HPPH[b]	1.043	1.03±0.01	This work
H_2PP (pyramidal)	1.426		
P_2H_3	1.557	1.74 eV (VDE)[c]	This work

[a]CCSD(T,FC)/aug-cc-pVTZ//B3LYP/aug-cc-pVTZ with zero-point energy corrections. Values in parenthesis are higher-level calculations from Ricca and Bauschlicher (Ref. 14).
[b]Tentative assignment of isomers, as discussed in text.
[c]Vertical detachment energy.

well-resolved peaks is ±0.005 eV (two combined standard uncertainties[24]). Atomic transition intensities and Franck–Condon factors for fitting molecular spectra are calculated using the PESCAL program described previously.[23,25,26]

Molecular structure and energy calculations are performed using GAUSSIAN 03.[27] Geometries and vibrational frequencies of the anions and neutral were calculated using density-functional theory (DFT) with Becke's three-parameter hybrid functional using the Lee–Yang–Parr correlation (B3LYP)[28] and with augmented correlation-consistent polarized valence triple-zeta (aug-cc-pVTZ) or quadruple-zeta (aug-cc-pVQZ) basis sets.[29–31] Electron affinities are calculated using coupled-cluster theory[32] at the coupled-cluster with single and double excitations and perturbative inclusion of triple excitations [CCSD(T)] level in single-point calculations at the geometries from DFT at the B3LYP level and unscaled harmonic-vibrational frequencies from DFT for zero-point energy corrections. The calculated electron affinities of the species discussed in this work are compared with experimental values from the literature and this work in Table I. These CCSD(T) electron affinity calculations use the frozen-core (FC) approximation and the triple-zeta basis set. Vibrational normal-mode coordinates and force constant matrices from the B3LYP/aug-cc-pVTZ calculations are used for Franck–Condon simulations of the spectra.

III. RESULTS AND DISCUSSION

A. Atomic phosphorus, P

The 363.8-nm photoelectron spectrum of P^- is displayed in Fig. 1. The electron affinity of phosphorus atom is precisely known from previous high-resolution photodetachment threshold measurements,[33,34] $EA_0(P)=0.7465\pm0.0003$ eV, as are the energy levels of the ^3P_J spin–orbit states of P^-, namely, $^3P_2$ (0 cm^{-1}), $^3P_1$ (181±2 cm^{-1}), and $^3P_0$ (263±2 cm^{-1}). The photoelectron spectrum exhibits transitions from these anion levels to the $^4S_{3/2}$ (0 cm^{-1}) and $^2D_{3/2}$ (11 361.02 cm^{-1}) and $^2D_{5/2}$ (11 376.63 cm^{-1}) levels[35] of the neutral atom. These transitions are assigned as indicated in Table II. The largest peaks in the two multiplets are due to the $P(^4S_{3/2})\leftarrow P^-(^3P_2)$ origin transition and the $P(^2D_{3/2})\leftarrow P^-(^3P_2)$ transition, respectively. The ^3P_J levels of P^- are clearly resolved in the spectrum, but the $^2D_{3/2}$ and $^2D_{5/2}$ levels of P are split by only 15.6 cm^{-1} (1.9 meV) and are not resolved.

Table II lists the calculated energies and relative intensities of the fine-structure transitions. The relative intensities are calculated in the *L-S* coupling approximation for one-electron detachment of a 3*p* electron using statistical factors and Clebsch–Gordan coefficients as described by Engelking and Lineberger.[36] The spectrum is fit by nonlinear least-

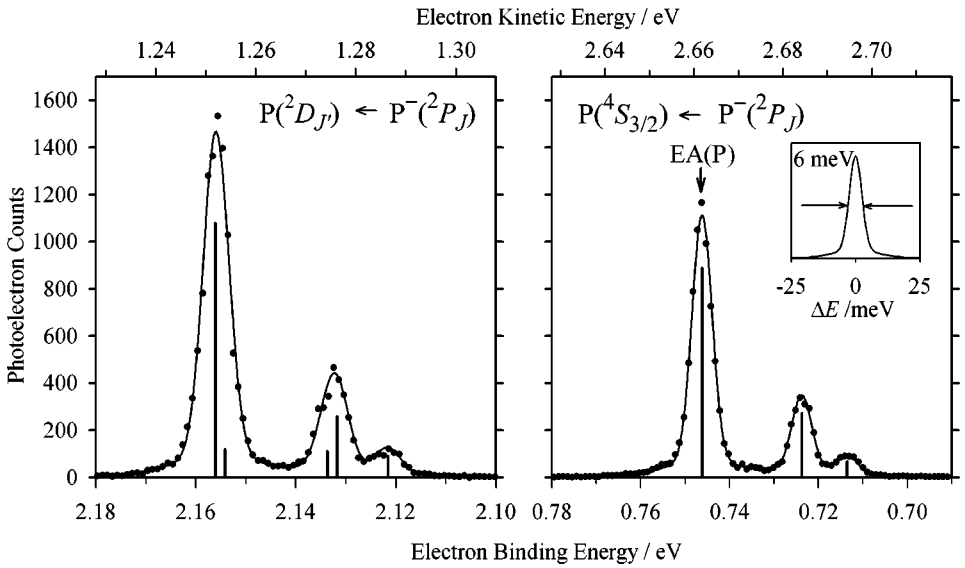

FIG. 1. Photoelectron spectrum of P^- at a laser wavelength of 363.8 nm ($h\nu=3.408$ eV). Photodetachment intensities (solid circles) are plotted as a function of the electron binding energy and electron kinetic energy (eBE$=h\nu-e$KE). The bars and curves show fits using calculated relative intensities with anion temperature of 390 K, as described in the text and listed in Table II. The inset shows the instrumental resolution function.

TABLE II. Fine-structure transitions for $P^- + h\nu \rightarrow P + e^-$.

			Relative intensity[a]		
Transition ($P \leftarrow P^-$)	Energy (cm^{-1})	*e*BE (eV)	Calc. ($T=\infty$)	Calc. ($T=390$ K)	Expt.
$^4S_{3/2} \leftarrow {}^3P_0$	-263 ± 2[b]	0.7139	0.111	0.055	0.06
$^4S_{3/2} \leftarrow {}^3P_1$	-181 ± 2[b]	0.7241	0.333	0.222	0.22
$^4S_{3/2} \leftarrow {}^3P_2$	0	0.7465[b]	0.556	0.723	0.72
$^2D_{3/2} \leftarrow {}^3P_0$	11098 ± 2[c]	2.1225	0.111	0.055	0.05
$^2D_{5/2} \leftarrow {}^3P_0$	11114 ± 2[c]	2.1245	0.000	0.000	···
$^2D_{3/2} \leftarrow {}^3P_1$	11180 ± 2[c]	2.1326	0.233	0.156	0.14
$^2D_{5/2} \leftarrow {}^3P_1$	11196 ± 2[c]	2.1346	0.100	0.067	0.08
$^2D_{3/2} \leftarrow {}^3P_2$	11361 ± 2[c]	2.1551	0.056	0.072	0.12
$^2D_{5/2} \leftarrow {}^3P_2$	11377 ± 2[c]	2.1571	0.500	0.650	0.61

[a]This work.
[b]Slater and Lineberger (Ref. 33), EA(P) = 0.7465 ± 0.0003 eV.
[c]Martin *et al.* (Ref. 35).

squares optimization, as shown in Fig. 1, with no adjustment of the predicted relative transition strengths. The typical instrumental resolution function obtained from the fit is a Gaussian distribution with a 6-meV full width at half maximum (FWHM) atop a second Gaussian "pedestal" of 22 -meV FWHM and 6% relative intensity. The best fit is obtained with an anion temperature of $T = 390 \pm 20$ K for the spin–orbit state populations. That is, the spin–orbit state populations of P^- are not completely equilibrated to the room-temperature flow tube buffer gas. The calculated relative fine-structure line strengths at this temperature are in excellent agreement with the directly measured intensities (right-most column of Table II), determined by fitting the spectra with the known transition energies but with transition intensities as additional adjustable parameters. The origin transition, $^4S_{3/2}P - {}^3P_2P^-$, is used to calibrate the absolute electron kinetic-energy scale of the electrostatic analyzer relative to the precise threshold photodetachment value.[33,34] A linear correction factor for the relative energy scale of $(0.6 \pm 0.2)\%$ is calibrated using the spacing between the $^4S_{3/2}P$ ground-state and the $^2D_{3/2}P$ excited-state transitions. When the anion spin–orbit energy splittings are treated as unknowns and the spectrum is fit with these as adjustable parameters, we find $E(^2P_0) = 265 \pm 5$ cm^{-1} and $E(^2P_1) = 181 \pm 5$ cm^{-1}.

B. Phosphinidene, PH

The photoelectron spectrum of PH^- is shown in Fig. 2. We observe transitions from the $X\,^2\Pi_j$ ground state of PH^- to the $X\,^3\Sigma^-$, $a\,^1\Delta$, and $b\,^1\Sigma^+$ states of PH. Each of these transitions is completely vertical—the $0 \leftarrow 0$ origins are observed, but no $1 \leftarrow 0$ or higher vibrational transitions or $0 \leftarrow 1$ hot bands. For all three electronic transitions, the electron is detached from one of the two nonbonding *p*-type orbitals centered on phosphorus. The three neutral electronic states represent the different ways of coupling the two electrons in these two orbitals. The absence of the $1 \leftarrow 0$ fundamental transitions places an upper limit of 0.02 for the Franck–Condon factors for each transition, limited by the base line noise level. Limits on the bond length of PH^- may be estimated from this experimental upper limit for the Franck–Condon factors. For this purpose we calculate Franck–Condon factors using the Morse oscillator approximation.[25,37] The spectroscopic bond lengths and vibrational constants for the neutral electronic states are listed in Table III.[38–46] For the anion vibrational constants, we use the theoretical values of Rosmus and Meyer[45] in Table III. These values agree with the less-precise experimental fundamental frequency of Zittel and Lineberger,[18] who were able to observe the $0 \leftarrow 1$ hot band in the photoelectron spectrum because of a higher anion temperature than is available with the present ion source. The Morse oscillator calculations show that a maximum Franck–Condon intensity of 0.02 corresponds to a maximum change in the bond length of 0.024 Å for the anion relative to any of the three observed electronic states of PH. Zittel and Lineberger[18] assumed that the bond length of PH^- is shorter than that of PH on the basis of comparisons with isoelectronic molecules, but *ab initio* calculations indicate that the anion is slightly longer. Rosmus and Meyer[45] and Meyer and Rosmus[47] find from coupled electron pair approach (CEPA) calculations that the ground-

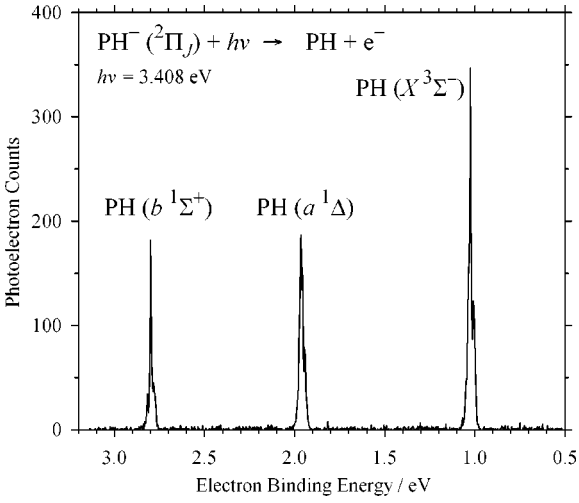

FIG. 2. Photoelectron spectrum of PH^- at a laser wavelength of 363.8 nm ($h\nu = 3.408$ eV). Photodetachment intensities (points) are plotted as a function of the electron binding energy. Transitions from the ground-state anion to the three lowest electronic states of PH are labeled. Each of the three electronic transitions show only the $0 \leftarrow 0$ vibrational origin transition.

TABLE III. Molecular constants of PH and PH^-.

Value	PH^- $X\,^2\Pi$	PH $X\,^3\Sigma^-$	PH $a\,^1\Delta$	PH $b\,^1\Sigma^+$
T_0	-1.027 ± 0.006 eV[a]	0	7558 ± 15 cm^{-1}[a]	$14\,310\pm30$ cm^{-1}[a]
			7555.08 cm^{-1}[b]	14 345 cm^{-1}[c]
r_e (Å)	$1.430<r_e<1.442$[a]	1.4222[d]	[1.420][e]	1.418[c]
r_0 (Å)		1.4329[b,d]	1.4305[b]	1.428[c]
ω_e (cm^{-1})	2248[f]	2363.8[d]	2415[g]	2403.0[c]
$\omega_e x_e$ (cm^{-1})	50[f]	43.9[d]	48[g]	42.0[c]
A (cm^{-1})	-185 ± 10[a]			

[a]This work.
[b]Reference 38.
[c]T_0 calculated from $T_e=14325.5\pm0.1$ cm^{-1} from Droege and Engelking (Ref. 40) and vibrational constants listed here. r_0 calculated from B_e and α_e. See also Refs. 41–44.
[d]Reference 39.
[e]Estimated from experimental r_0 by interpolation between other states.
[f]Theoretical values used for Franck–Condon calculations (Ref. 45).
[g]Theoretical values used for Franck–Condon calculations (Ref. 46).

state bond length is 0.015 Å longer in the anion, while our density-functional theory calculations at the B3LYP/aug-cc-pVQZ level give 0.011 Å. These values are completely consistent with our experimental upper limit of 0.024 Å. Taking the shortest of the neutral states,[40] $r_e=1.418$ Å for PH $b\,^1\Sigma^+$, our maximum bond-length change yields an upper limit of $r_e<1.442$ Å for PH^- $X\,^2\Pi_J$. The minimum change of 0.008 Å found by Zittel and Lineberger[18] from the intensity of the $0\leftarrow1$ hot band of the PH $X\,^3\Sigma^-\leftarrow PH^-$ $X\,^2\Pi$ transition gives a lower limit of $r_e>1.430$ Å. Thus, the bond length of the anion is fairly tightly established as $1.430\ \text{Å}\leqslant r_e\leqslant1.442$ Å, in excellent agreement with the CEPA theoretical value[45] of 1.441 Å and our calculation of 1.439 Å at the B3LYP/aug-cc-pVQZ level.

Figure 3 presents each electronic transition in the photoelectron spectrum of PH^- on an expanded scale, showing that these transitions are structured. The structure arises from the spin–orbit splitting of the $^2\Pi_{3/2}$ and $^2\Pi_{1/2}$ states of PH^- and from the contours of partially resolved rotational branches, which were not resolved in the previous photoelectron spectra.[18] To simulate the contours, line positions and line strengths are calculated for $[PH(^{1,3}\Sigma)+e^-]\leftarrow PH^-(^2\Pi_j)$ and $[PH(^1\Delta)+e^-]\leftarrow PH^-(^2\Pi_j)$ absorption transitions using the DIATOMIC program[48] with the rotational and spin–orbit coupling constants in Table III, and then convolved over the instrumental resolution function obtained from the atomic P^- spectrum. The spin–orbit constant for the anion and the anion temperature are obtained by manually adjusting the values in DIATOMIC until a reasonable match to the observed contours is obtained. We obtain good fits with $T=300$ K and $A(^2\Pi_j)=-185\pm10$ cm^{-1}. As shown in Fig. 3, very good but not perfect agreement with the observed contours is obtained. The small deviations may arise from the approximation of treating the photodetachment process as an absorption transition (i.e., neglecting the detailed interaction of the outgoing electron with the states of the neutral) or the approximation that the rotational and spin–orbit temperatures of the anion are identical. Modeling with values of the spin–orbit splitting outside this -185 ± 10 cm^{-1} range results in visually degraded fits to the main branches. To our knowledge, this result is the first experimental measurement of the spin–orbit splitting in PH^-. It is in excellent agreement with the theoretical value of -185.7 cm^{-1} calculated by relativistic self-consistent-field methods.[49] The rotationless origins for each electronic transition are marked by vertical bars in Fig. 3. The energies of these origin transitions give the adiabatic

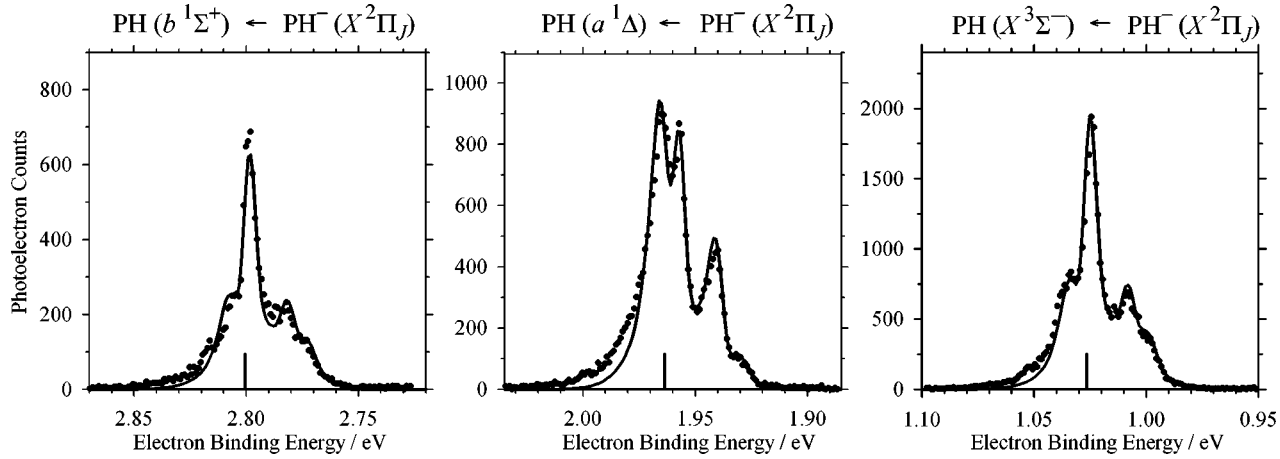

FIG. 3. Expanded portions of the photoelectron spectrum of PH^- showing the partially resolved rotational and spin–orbit state contours of the three electronic transitions. The points represent the photodetachment intensities and the curves show the calculated rotational and spin–orbit transitions convolved over the instrumental resolution function, as described in the text. The vertical bars mark the rotationless origins of each transition.

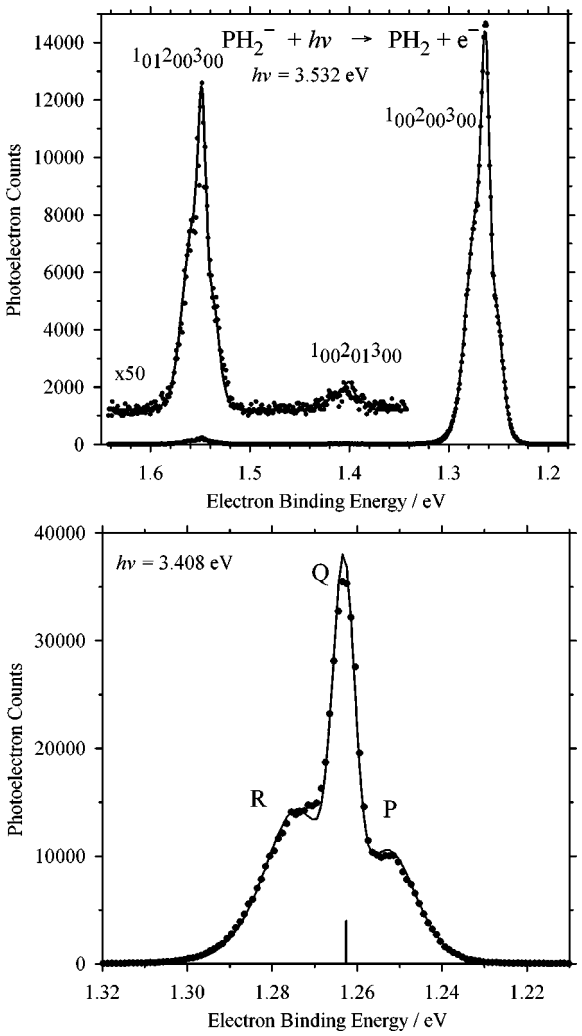

FIG. 4. Photoelectron spectra of PH_2^-. (a) Full spectrum at a laser wavelength of 351.1 nm ($h\nu$=3.531 eV) plotted as a function of the electron binding energy. The points represent the photodetachment intensities and the line is a Franck–Condon fit, as discussed in the text. The region including the symmetric stretch and bending transitions is multiplied by a factor of 50 and offset from the lower axis. (b) Spectrum of the origin transition at a laser wavelength of 363.8 nm ($h\nu$=3.408 eV) and with higher resolution conditions than in part (a). Photodetachment intensities (points) are compared with the calculated rotational contour (line). The unresolved contours of the *P*, *Q*, and *R* branches are labeled. The vertical bar marks the rotationless origin.

electron binding energy for each electronic state. The resulting value for the adiabatic electron affinity is $EA_0(PH\ X\ ^3\Sigma^-) = 1.027 \pm 0.006$ eV, which is in complete agreement with the previous experimental value of 1.028 ± 0.010 eV.[18] The measured electronic term energies are $T_0(PH\ a\ ^1\Delta) = 0.953 \pm 0.003$ eV or 7560 ± 20 cm^{-1} and $T_0(PH\ b\ ^1\Sigma^+) = 1.774 \pm 0.005$ eV or 14310 ± 40 cm^{-1}. These energies agree with literature values of $T_0(PH\ a\ ^1\Delta) = 7555.1$ cm^{-1} and $T_0(PH\ b\ ^1\Sigma^+) = 14345$ cm^{-1} from electronic spectroscopy (Table III).[38,40]

C. Phosphino radical, PH_2

Figure 4(a) shows the vibrational transitions of the $PH_2(X\ ^2B_1) \leftarrow PH_2^-(X\ ^1A_1)$ band in the photoelectron spectrum of PH_2^-. No other transitions are observed in the energy range of the experiment. The spectrum is nearly vertical, dominated by the $0 \leftarrow 0$ origin transition, consistent with detachment of the electron from a nonbonding phosphorus *p*-type orbital. A weak $1 \leftarrow 0$ transition of the υ_1 symmetric stretch vibration is clearly observed and a slight rise above the background is observed at the expected position of the $1 \leftarrow 0$ transition of the υ_2 bending vibration. The asymmetric stretch mode is not active by symmetry selection rules, and the relatively high anion frequencies and small Franck–Condon factors suppress the hot bands. The origin transition and symmetric stretch fundamental transition exhibit partially resolved rotational contours with a central *Q* branch peak and adjacent *P* and *R* branches, as shown in the expanded plot of the origin transition in Fig. 4(b).

TABLE IV. Molecular constants for PH_2 and PH_2^-.

Constant	PH_2^-[a]	PH_2
A (cm^{-1})	8.96	9.113[b]
B (cm^{-1})	7.76	8.083[b]
C (cm^{-1})	4.16	4.214[b]
r (Å)	$r' + (0.016 \pm 0.004) \approx 1.439$	1.423[b]
θ (°)	$\theta' + (0.6 \pm 0.2) \approx 92.3$	91.7[b]
ν_1 (cm^{-1})	1060[c]	1101.4[c]
ν_2 (cm^{-1})	2221[d]	2295 ± 15[a]
		2310 ± 2[e]
ν_3 (cm^{-1})	2225[d]	2336[d]
EA (eV)		1.263 ± 0.006[a]

[a]This work except as noted. Rotational constants are calculated from the estimated geometry neglecting the inertial defect.
[b]Reference 51.
[c]References 53 and 55.
[d]Frequencies calculated at the B3LYP/aug-cc-pVTZ level with a scaling factor of 0.98.
[e]References 54 and 55.

To model the rotational contour, the photodetachment transition is treated as a two-step process,[50] $PH_2^-(X\ ^1A_1) \rightarrow PH_2^{-*}(^1B_1) \rightarrow PH_2(X\ ^2B_1) + e^-(ks)$. The virtual intermediate anion state represents the PH_2^- anion with the extra electron in a continuum *s* orbital. As described in a previous work on the isovalent anion NH_2^-,[50] the rotational energy levels and transition intensities are calculated for an asymmetric rotor using type-*C* selection rules. Rotational constants are known for the neutral and are presented in Table IV.[1,51–53] For the anion we used calculated geometries for initial fits, but the contours shown in Fig. 4 use the rotational constants in Table IV obtained from our Franck–Condon analysis described below. A temperature of 300 K was used for Boltzmann rotational energy-level populations and the calculated lines are broadened by the instrumental resolution function obtained from the atomic phosphorus spectrum. This simulated contour agrees well with the experiment, as shown in Fig. 4(b). The binding energy of the rotationless origin marked in Fig. 4(b) represents the measured adiabatic electron affinity, $EA_0(PH_2) = 1.263 \pm 0.006$ eV, in agreement with the previous photoelectron spectroscopy value[18] of 1.271 ± 0.010 eV.

The position of the $1 \leftarrow 0$ transition of the symmetric stretch gives a vibrational frequency for neutral PH_2 of 2295 ± 15 cm^{-1}, in reasonable agreement with 2310 ± 2 cm^{-1} from a high-temperature Raman spectrum[54] (obtained by

subtracting the PH_3 signal from the spectrum of PH_2 and PH_3). The bending vibration is too weak for a precise determination of its frequency; we use the spectroscopic value[53,55] of 1101.4 cm^{-1}. By comparison with these experimental frequencies, an empirical scaling factor of 0.98 is determined for frequencies calculated by the B3LYP/aug-cc-pVTZ method. These scaled frequencies for the anion and the inactive symmetric stretch are listed in Table IV. To model the intensities, Franck–Condon factors are calculated in the harmonic-oscillator approximation using methods described previously.[26] Duschinsky rotation is included using normal coordinate vectors from the B3LYP/aug-cc-p-VTZ frequency calculations, but the Duschinsky rotation effect is minor for this system. The geometry displacements between the known values for the neutral (Table IV)[51] and the anion are found by fitting the Franck–Condon intensities. The Franck–Condon fit can establish the magnitude but not the sign of the changes in the bond length and angle. Calculations show that both increase from neutral to the anion. Using the calculated geometries to assign the direction of the change, we find that the bond length in the anion is 0.016 ± 0.004 Å longer than in the neutral and that the bond angle is $0.6° \pm 0.2°$ wider. Using geometry values for the neutral from Chen *et al.*,[51] we can estimate geometries and rotational constants for PH_2^-, as listed in Table IV.

D. Identification of $P_2H_n^-$ species

The $P_2H_n^-$ species are incompletely resolved in the mass spectrum. Survey photoelectron spectra, taken by adjusting the setting of the Wien filter to the low- or high-mass side of the $P_2H_n^-$ peak, are compared in Figs. 5(a) and 5(b). These spectra show that at least two different molecular anions are present. The major species in Fig. 5(a) has an origin peak at an electron binding energy of about 1.52 eV and is on the low-mass side of the peak. Three additional transitions arise when the mass setting is moved to the higher-mass side of the peak, as shown in Fig. 5(b). To identify the major transitions in Figs. 5(a) and 5(b), we compare them with simulated spectra for P_2^-, P_2H^-, $P_2H_2^-$, and $P_2H_3^-$ in Figs. 5(c)–5(h). The simulated spectra use B3LYP/aug-cc-pVTZ geometries, frequencies, and normal-mode vectors, with electron affinities calculated at the CCSD(T)/aug-cc-pVTZ//B3LYP/aug-cc-pVTZ level. The Franck–Condon profiles are calculated in the harmonic-oscillator approximation with full treatment of Duschinsky rotation.[25,26]

Several low-lying electronic states and isomers of P_2H_2 and $P_2H_2^-$ exist, as previously studied by Schaefer and co-workers.[9–11] Our theoretical calculations generally agree with those results; here we use the CCSD(T)/aug-cc-pVTZ//B3LYP/aug-cc-pVTZ relative energies as shown in Fig. 6 for consistent comparisons. The Franck–Condon simulations for *trans*-$HPPH^-$ and *cis*-$HPPH^-$ are shown in Figs. 5(e) and 5(f), respectively. The *trans* isomer is the ground doublet state of the anion and the neutral singlet ground state, but the *cis* isomer is only 0.10 eV higher for the anion and 0.14 eV higher for the neutral according to the calculations. The stable geometry of the triplet excited state of neutral HPPH is nonplanar (skewed geometry), with a dihedral angle of

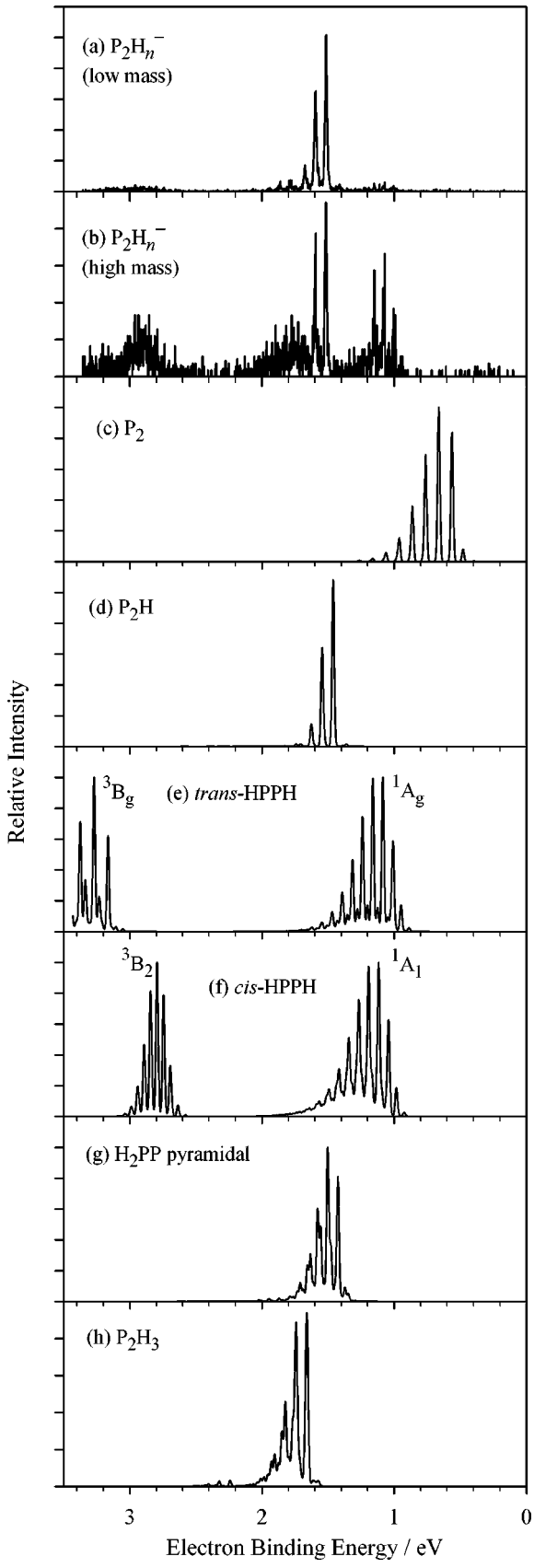

FIG. 5. Comparison of experimental and simulated photoelectron spectra of $P_2H_n^-$ species. Normalized band intensities are plotted as a function of the electron binding energy. (a) Experimental spectrum on the low-mass side of the mass peak. (b) Experimental spectrum on the high-mass side of the mass peak. (c)–(h) Simulated Franck–Condon profiles for the labeled species, as discussed in the text.

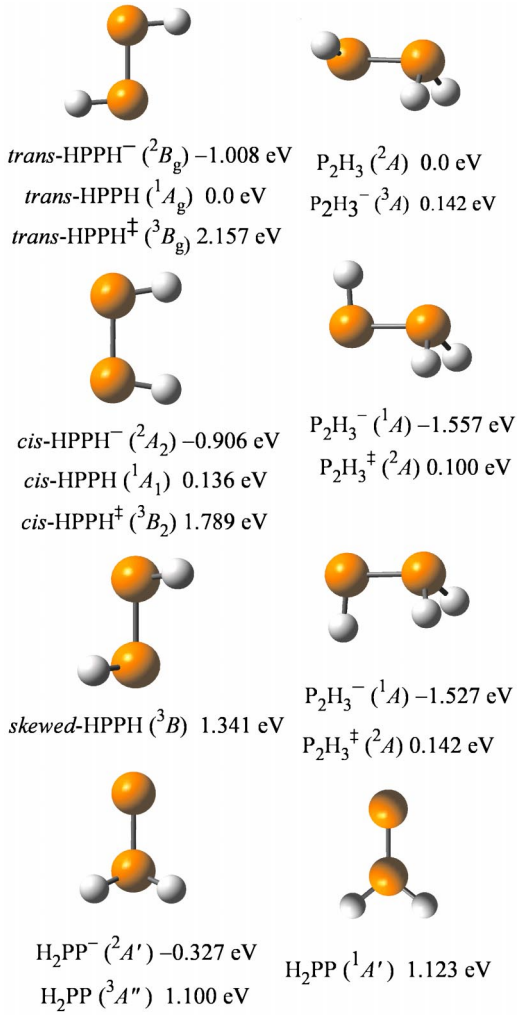

FIG. 6. Structures of low-lying isomers and electronic states of P_2H_2, P_2H_3, and their anions. Energies in eV relative to the ground-state neutrals are calculated at the CCSD(T)/aug-cc-pVTZ//B3LYP/aug-cc-pVTZ level. The structures represent minima on the potential-energy surface except for transition states marked with a superscript dagger, which have one imaginary frequency.

92°. The *cis* and *trans* isomers on the neutral triplet surface represent transition state geometries for the rotation around the PP bond of the skewed, nonplanar HPPH. The geometry difference between the anion (either *trans* or *cis*) and the nonplanar neutral triplet is thus quite large and the Franck–Condon factors in the harmonic approximation are not meaningful. The simulations in Fig. 5 for *cis*-$HPPH^-$ and *trans*-$HPPH^-$ instead show the vertical transitions to the *cis*-HPPH and *trans*-HPPH triplet transition states, respectively, obtained by simply ignoring the mode with imaginary frequency in the upper state. That is an oversimplification; these simulations are intended merely to show the regions where the transition to the neutral triplet surface might occur. The relative intensities of the two electronic transitions are arbitrarily normalized. The pyramidal H_2PP^- anion is 0.68 eV higher than the ground-state *trans*-$HPPH^-$. The Franck–Condon simulation for pyramidal H_2PP^- to the triplet ground-state neutral is shown in Fig. 5(g). Singlet H_2PP is calculated to be only 0.023 eV higher than the triplet, but it is planar and would therefore have poor Franck–Condon

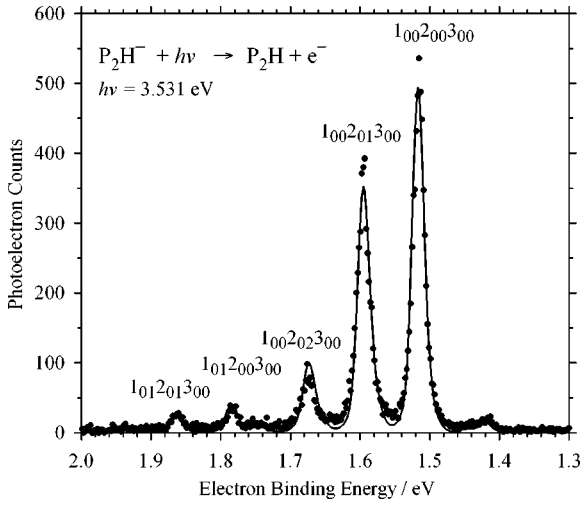

FIG. 7. Photoelectron spectrum of P_2H^- at a laser wavelength of 351.1 nm ($h\nu$=3.531 eV). Photodetachment intensities (points) are plotted as a function of the electron binding energy. The solid line is the Franck–Condon fit described in the text. The labels indicate the vibrational transition assignments for the ν_1 (PH stretch), ν_2 (PPH bend), and ν_3 (PP stretch) modes.

overlap with the ground-state anion. Barriers for interconversion of the neutral P_2H_2 isomers are expected to be high.[12,13]

The geometries of the calculated low-energy isomers of $P_2H_3^-$ and P_2H_3 are also shown in Fig. 6. Compared with the lowest-energy singlet H_2PPH^- anion geometry with C_s symmetry, the neutral molecule is asymmetric with the PPH plane containing the lone hydrogen rotated out of the anionic C_s plane by about 72°. The singlet anion has two nearly degenerate conformations in C_s symmetry, which correspond to saddle points on the neutral doublet surface. The triplet anion has the same asymmetric geometry as the neutral, but is unbound with respect to electron detachment. Because the anion has poor Franck–Condon overlap with the ground-state neutral, the harmonic approximation for Franck–Condon factors is not useful. In Fig. 5(h), we instead plot the simulated spectrum for vertical transitions from the C_s anions to the C_s saddle points on the neutral surface, with the two anion conformations weighted for a 300-K population. The actual spectrum to the asymmetric neutral would be expected to be in the same energy region but with greater broadening because of the neglected displacement in the H_2P-PH internal rotation coordinate.

We now compare the simulated spectra in Figs. 5(c)–5(h) to the experimental spectra in Figs. 5(a) and 5(b) to aid species assignments. It is clear that the major observed transition near eBE=1.5 eV is P_2H^-, as simulated in Fig. 5(d). This band is shown in Fig. 7 under conditions that minimize interferences and is considered in detail in Sec. III E. No transitions matching P_2^- are observed, but the simulated spectrum in Fig. 5(c) is similar to the experimental spectra reported by Snodgrass *et al.*[56] and by Jones *et al.*,[57] with $EA(P_2)=0.589\pm0.025$ eV.[56] The observed band near eBE=1.0 appears to be due to *trans*-$HPPH^-$ or *cis*-$HPPH^-$. Figure 8 shows the $HPPH^-$ transition under conditions where P_2H^- is suppressed; this spectrum is considered further below. Judging by the intensities as the mass setting is varied, the band near eBE=2.9 eV likely arises from anions of the

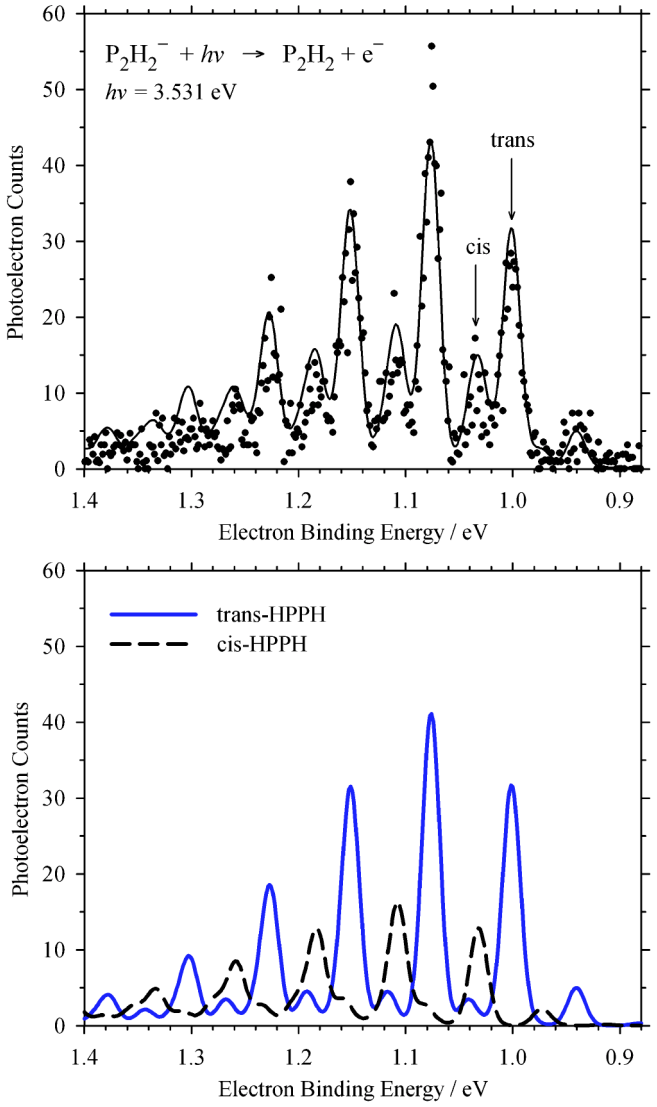

FIG. 8. (a) Experimental photoelectron spectrum of $HPPH^-$ at a laser wavelength of 351.1 nm ($h\nu$=3.531 eV). Photoelectron counts (points) are plotted as a function of the electron binding energy. The arrows indicate the origins of the PP-stretch mode progressions, tentatively assigned to *trans*-HPPH and *cis*-HPPH as discussed in the text. (b) Franck–Condon fits for the primary vibrational progression assigned to *trans*-$HPPH^-$ (solid line) and to the secondary vibrational progression assigned to *cis*-$HPPH^-$ (dashed line). The solid line in part (a) is the sum of the fits for these two isomers.

same mass as the *e*BE=1.0 eV transition, i.e., P_2H_2. We tentatively assign this band to triplet HPPH, which as discussed above would be a transition to the triplet surface in the region of the *cis*- or *trans*-HPPH transition states for isomerization between the two possible nonplanar HPPH geometries.

The final band observed for the higher-mass $P_2H_n^-$ species is a weak transition that peaks at *e*BE=1.74 eV and that partially overlaps the stronger P_2H^- band, as shown in Fig. 5(b). The two candidates for its assignment are pyramidal H_2PP^- and H_2PPH^-. We tentatively assign this transition as H_2PPH^- because the calculated energy matches better than for pyramidal H_2PP^- and because it would be surprising to have the highly excited H_2PP^- isomer present in the ion beam. No origin transition can be discerned, which is consistent with a broad, nonvertical transition as expected from H_2PPH^- to the asymmetric H_2PPH neutral. This band is too weak for more detailed analysis.

E. Diphosphenyl radical, P_2H

Figure 7 shows the spectrum of the P_2H ($^2A'$) $\leftarrow P_2H^-(^1A')$ transition and a Franck–Condon fit with optimized displacements and neutral frequencies. The spectrum shown was taken on the low-mass side of the $P_2H_n^-$ mass peak and is predominantly due to P_2H^-. Two vibrational progressions can be identified. The calculations for neutral P_2H give frequencies of 2267 cm^{-1} (PH stretch), 666 cm^{-1} (PPH bend), and 611 cm^{-1} (PP stretch). The first two frequencies have the largest calculated normal-mode displacements between the singlet anion and the neutral, and can therefore be assigned as the observed modes. We therefore assign the 2160 ± 30 cm^{-1} progression to the PH stretch (ν_1) and the 630 ± 20 cm^{-1} progression to the PPH bend (ν_2). For calculating the Franck–Condon fits, the frequencies for unobserved modes are fixed at the calculated values, scaled by 95% to match the two experimental frequencies. The peak profiles are simulated by treating P_2H and P_2H^- as asymmetric rotors and convoluting over the instrumental resolution function. The overall peak contour has a full width at half maximum of 20 meV, and the effective rotational correction of the origin peak position is −2 meV. The electron affinity from the optimized fits is $EA_0(P_2H)=1.514\pm0.010$ eV. To our knowledge, there are no previous experimental reports of this electron affinity.

Because the PP-stretching mode is not observed, the exact geometry change cannot be derived from the data. We obtain approximate values by fixing the displacement for that mode at the (small) calculated value, and using the Franck–Condon intensities to fit the displacements in the other two modes. This gives estimates of an increase of 0.023 Å for the PP distance, an increase of 0.068 Å for the PH distance, and an increase of 8° in the PPH angle from the neutral to the anion. The calculated neutral geometry is $r(PP)=2.007$ Å, $r(PH)=1.435$ Å, and $\alpha=98°$; experimental values are unknown.

F. Diphosphene, HPPH

The experimental spectrum of the $HPPH^-$ band is shown on an expanded scale in Fig. 8. The signal is weak, but there is a clear vibrational progression starting at an origin at *e*BE=1.00 eV with a frequency of about 600 cm^{-1}. As noted above, the *trans*-$HPPH^-$ and *cis*-$HPPH^-$ isomers have very similar calculated energies, frequencies, and simulated Franck–Condon profiles. Therefore, a definitive isomeric assignment of the experimental spectrum is not possible. The major vibrational progression can be fit starting with the simulated spectra of either isomer and making minor adjustments to the PP-stretch mode frequency (calculated as 616 cm^{-1} in *trans*-HPPH and 603 cm^{-1} in *cis*-HPPH) and geometry displacements. The other two active, totally symmetric vibrational modes—the PH symmetric stretches with calculated frequencies of 2335^{-1} and 2366 cm^{-1} for *trans* and *cis*, respectively, and the PPH symmetric in plane bends

TABLE V. Derived thermochemical values.

	RH			
Value	PH	PH_2	PH_3	Ref.
$EA_0(R)$ (eV)	0.7465±0.0003	1.027±0.006	1.263±0.006	Expt.[a]
	0.734	1.026	1.271	Theory[b]
D_0(R-H) (kJ mol^{-1})	293.3±2.1	⩾312.5±2.1	⩽345.0±1.9	Expt.[c]
	293.0	317.5	339.6	Theory[b]
$\Delta_{acid}H_0$(RH) (kJ mol^{-1})	1533.3±2.1	⩾1525.6±2.2	⩽1535.2±2.0	Expt.[d]
	1534.6	1530.9	1529.4	Theory[b,d]
$\Delta_{acid}H_{298}$(RH) (kJ mol^{-1})	1537.6±2.1	⩾1530.9±2.2	⩽1541.3±2.0	Expt.[e]
$\Delta_{acid}S_{298}$(RH) (J mol^{-1} K^{-1})	80.1±2	96.7±2	105.9±2	Expt.[e]
$\Delta_{acid}G_{298}$(RH) (kJ mol^{-1})	1513.7±2.2	⩾1502.1±2.2	⩽1509.7±2.1	Expt.[f]
			1520±8.4	Expt.[g]

[a]From Table I.
[b]CCSD(T) with complete basis-set extrapolation, zero-point energy, and spin–orbit corrections from Ricca and Bauschlicher (Ref. 14). Gas-phase phase acidities derived using IE(H)=0.5 hartree.
[c]Berkowitzand co-workers (Refs. 58–62).
[d]$\Delta_{acid}H(RH)=D(RH)+IE(H)-EA(R)$.
[e]Thermal enthalpy correlations and entropies calculated using the harmonic-oscillator, rigid-rotor approximations: $\Delta H_{298}=\Delta H_0+\int_0^{298}\Delta C_p dT$ and $\Delta S_{298}=\int_0^{298}(\Delta C_p/T)dT$.
[f]$\Delta G=\Delta H-T\Delta S$.
[g]Ion cyclotron resonance equilibrium (Ref. 65).

at 970 and 741 cm^{-1}—have small calculated Franck–Condon factors and are not observed. The activity of the PP-stretch mode results from the removal of an electron from the highest-occupied molecular orbital in the anion, which is essentially a phosphorus out-of-plane $p\pi^*$ antibonding orbital. The *trans*-HPPH parameters do provide a slightly better fit, consistent with the 0.1-eV lower energy calculated for *trans*-$HPPH^-$ compared with *cis*-$HPPH^-$, but either fit of the major progression is acceptable given the quality of the data. However, there is an additional weaker secondary vibrational progression that is not reproduced by either simulation. It has an apparent origin at *e*BE=1.03 eV and a frequency also of about 600 cm^{-1}. The 240-cm^{-1} spacing between the origin of the major progression at 1.00 eV and the peak at 1.03 eV is too small to match any of the vibrational modes of either *trans*-HPPH or *cis*-HPPH. Therefore, we provisionally assign this progression to the isomer *other* than the one responsible for the major progression. Using the theoretical energies as a guide, we can tentatively identify the major progression as *trans*-$HPPH^-$ with EA_0(*trans*-HPPH) =1.00±0.01 eV and the secondary progression as *cis*-$HPPH^-$ with EA_0(*cis*-HPPH)=1.03±0.01 eV. Overlap of the two isomer transitions and the weak signal intensity preclude further analysis.

A more remote possibility for the assignment of the secondary progression is to the $1\leftarrow 1$ hot sequence band of the out-of-plane bending mode, noting that $\Delta v=0$ transitions are allowed for nontotally symmetric modes. The out-of-plane bend exhibits a large calculated frequency change from 449 cm^{-1} (289 cm^{-1}) in the anion to 775 cm^{-1} (699 cm^{-1}) in the neutral for the *trans*(*cis*) isomer. These transitions are seen in the simulation in Fig. 8(b) for the *trans* isomer as small peaks at *e*BE=1.042, 1.117, and 1.192 eV. Fitting the intensities and transition energies of this mode to the experimental peaks would require a shift of frequency of 8% (21% for *cis*) from the calculated value for the neutral *and* a non-Boltzmann vibrational population of the anion, at least in the harmonic-oscillator approximation. Therefore, this assignment is less satisfactory. Observation of these sequence transitions in a higher-resolution experiment could help confirm the identities of the isomers.

G. Thermochemistry

The electron affinities determined in this work are collected in Table I and compared with literature and calculated values. The gas-phase acidities of PH, PH_2, and PH_3 can be derived from the electron affinities reported here and the bond dissociation energies from Berkowitz *et al.*[58–62] using the negative-ion thermochemical cycle, $\Delta_{acid}H(RH)=D(RH)-EA(R)+IE(H)$, where the ionization energy of hydrogen is IE(H)=1312.05 kJ/mol.[63] These derivations are summarized in Table V. The experimental P–H bond dissociation energies of PH_3 and PH_2 rely on the threshold photoionization appearance energy of PH_2^+ from PH_3, which is (strictly) an upper limit.[58,59] Therefore, $D_0(H_2P-H)$ and $D_0(HP-H)$ are upper and lower limits, respectively, and a decrease in the value of $D_0(H_2P-H)$ implies an equal increase in $D_0(HP-H)$. Thermal enthalpy and entropy corrections have been applied in the harmonic-oscillator, rigid-rotor approximations using experimental parameters reported in Tables III and IV or B3LYP/aug-cc-pVTZ calculated values.

For PH_3, the gas-phase acidity of $\Delta_{acid}G_{298}$ ⩽1509.7±2.1 kJ/mol derived in Table V may be compared with an ion cyclotron resonance equilibrium measurement[64,65] of 1520±8.4 kJ/mol. With just touching error bars, these values are not in good agreement, but the experimental discrepancy of 29 kJ/mol in the negative-ion cycle for PH_3 that was noted by Bartmess[65] has been diminished.

The experimental electron affinities, bond dissociation energies, and gas-phase acidities are compared in Table V

with theoretical calculations reported by Ricca and Bauschlicher, Jr.[14] at the CCSD(T) level with complete basis-set extrapolation, zero-point energy corrections, and spin–orbit energy corrections. The theoretical values for the three electron affinities and for $D_0(\mathrm{P-H})$ are in superb agreement with experiment, within about 1 kJ/mol. The theoretical values of $D_0(\mathrm{HP\text{-}H})$ and $D_0(\mathrm{H_2P\text{-}H})$ are higher and lower by about 5 kJ/mol than the experimental lower and upper limits, respectively, which is consistent and implies that the experimental upper limit for the appearance energy[58,59] of PH_2^+ from PH_3 could be higher than the true value by that amount. The deviations between theory and experiment for the gas-phase acidities in Table V mirror those of the dissociation energies.

IV. CONCLUSION

We have reported electron affinities and other molecular parameters for small phosphorus hydride species. Simulated Franck–Condon profiles using geometries and normal modes from density-functional theory have proven very useful for identifying the bands in photoelectron spectra. Without high-quality theoretical input, the assignment of the $P_2H_n^-$ species would be difficult. Accurate molecular structure calculations and the development of software for routine Franck–Condon simulations of photoelectron spectra using calculated vibrational force fields make the spectroscopic assignments possible.

ACKNOWLEDGMENTS

We thank Charles W. Baushlicher, Jr. and Joseph Berkowitz for helpful correspondence regarding their work. This work has been supported by the U.S. Department of Energy, Office of Science, Office of Basic Energy Science, Chemical Sciences, Geosciences, and Biosciences Division (KME); and by the National Science Foundation, Grant Nos. CHE-0201848 and PHY-0096822 (WCL).

[1] L. Margulès, E. Herbst, V. Ahrens, F. Lewen, G. Winnewisser, and H. S. P. Müller, J. Mol. Spectrosc. **211**, 211 (2002).
[2] R. J. Morton and R. I. Kaiser, Planet. Space Sci. **51**, 365 (2003).
[3] O. Korobeinichev, T. Bolshova, V. Shvartsberg, and A. Chernov, Combust. Flame **125**, 744 (2001).
[4] N. L. Haworth and G. B. Bacskay, J. Chem. Phys. **117**, 11175 (2002).
[5] Y. Hirota and T. Kobayashi, J. Appl. Phys. **53**, 5037 (1982).
[6] A. Robertson and A. S. Jordan, J. Vac. Sci. Technol. B **11**, 1041 (1993).
[7] T. Sugino, M. Maeda, K. Kawarai, and J. Shirafuji, J. Cryst. Growth **166**, 628 (1996).
[8] M. W. Schmidt and M. S. Gordon, Inorg. Chem. **25**, 248 (1986).
[9] T. L. Allen, A. C. Scheiner, Y. Yamaguchi, and H. F. Schaefer, III, Chem. Phys. Lett. **121**, 154 (1985).
[10] T. L. Allen, A. C. Scheiner, Y. Yamaguchi, and H. F. Schaefer, III, J. Am. Chem. Soc. **108**, 7579 (1986).
[11] T. L. Allen, A. C. Scheiner, and H. F. Schaefer, III, J. Phys. Chem. **94**, 7780 (1990).
[12] M. T. Nguyen and T.-K. Ha, Chem. Phys. Lett. **158**, 135 (1989).
[13] K. Ito and S. Nagase, Chem. Phys. Lett. **126**, 531 (1986).
[14] A. Ricca and C. W. Bauschlicher, Jr., Chem. Phys. Lett. **285**, 455 (1998).
[15] Z. Gan, K. Su, Y. Wang, and Z. Wen, Chem. Phys. **228**, 31 (1998).
[16] M. Baudler and K. Glinka, Chem. Rev. (Washington, D.C.) **94**, 1273 (1994).
[17] R. Rackwitz, D. Feldmann, H. J. Kaiser, and E. Heinicke, Z. Naturforsch. A **32**, 594 (1977).
[18] P. F. Zittel and W. C. Lineberger, J. Chem. Phys. **65**, 1236 (1976).
[19] K. C. Smyth and J. I. Brauman, J. Chem. Phys. **56**, 1132 (1972).
[20] D. G. Leopold, K. K. Murray, A. E. Stevens Miller, and W. C. Lineberger, J. Chem. Phys. **83**, 4849 (1985).
[21] K. M. Ervin and W. C. Lineberger, in *Advances in Gas Phase Ion Chemistry*, edited by N. G. Adams and L. M. Babcock (JAI, Greenwich, CT, 1992), Vol. 1, p. 121.
[22] K. M. Ervin, J. Ho, and W. C. Lineberger, J. Chem. Phys. **91**, 5974 (1989).
[23] K. M. Ervin, I. Anusiewicz, P. Skurski, J. Simons, and W. C. Lineberger, J. Phys. Chem. A **107**, 8521 (2003).
[24] B. N. Taylor and C. Kuyatt, NIST Technical Note No. 1297, 1994, http://physics.nist.gov/Document/tn1297.pdf
[25] K. M. Ervin, Fortran program PESCAL, University of Nevada, Reno 2004.
[26] K. M. Ervin, T. M. Ramond, G. E. Davico, R. L. Schwartz, S. M. Casey, and W. C. Lineberger, J. Phys. Chem. A **105**, 10822 (2001).
[27] M. J. Frisch, G. W. Trucks, H. B. Schlegel *et al.*, Gaussian 03, Revision B.02, Gaussian, Inc., Pittsburgh, PA, 2003.
[28] A. Becke, J. Chem. Phys. **98**, 5648 (1993).
[29] T. H. Dunning, Jr., J. Chem. Phys. **90**, 1007 (1989).
[30] R. A. Kendall, T. H. Dunning, Jr., and R. J. Harrison, J. Chem. Phys. **96**, 6792 (1992).
[31] D. E. Woon and T. H. Dunning, Jr., J. Chem. Phys. **98**, 1358 (1993).
[32] J. A. Pople, M. Head-Gordon, and K. Raghavachari, J. Chem. Phys. **87**, 5968 (1987).
[33] J. Slater and W. C. Lineberger, Phys. Rev. A **15**, 2277 (1977).
[34] T. Andersen, H. K. Haugen, and H. Hotop, J. Phys. Chem. Ref. Data **28**, 1511 (1999).
[35] W. C. Martin, R. Zalubas, and A. Musgrove, J. Phys. Chem. Ref. Data **14**, 751 (1985).
[36] P. C. Engelking and W. C. Lineberger, Phys. Rev. A **19**, 149 (1979).
[37] J. Ho, K. M. Ervin, and W. C. Lineberger, J. Chem. Phys. **93**, 6987 (1990).
[38] M. Beutel, K. D. Setzer, O. Shestakov, and E. H. Fink, Chem. Phys. Lett. **249**, 183 (1996).
[39] R. S. Ram and P. F. Bernath, J. Mol. Spectrosc. **176**, 329 (1996).
[40] A. T. Droege and P. C. Engelking, J. Chem. Phys. **80**, 5926 (1984).
[41] G. Di Stefano, M. Lenzi, A. Margani, and C. Nguyen Xuan, J. Chem. Phys. **68**, 959 (1978).
[42] C. Nguyen Xuan, M. Tamanini, G. Di Stefano, and A. Margani, Gazz. Chim. Ital. **116**, 243 (1986).
[43] G. Di Stefano, M. Lenzi, G. Piciacchia, and A. Ricci, Chem. Phys. **165**, 201 (1992).
[44] M. N. R. Ashfold, R. N. Dixon, and R. J. Stickland, Chem. Phys. Lett. **1984**, 226 (1984).
[45] P. Rosmus and W. Meyer, J. Chem. Phys. **69**, 2745 (1978).
[46] P. J. Bruna, G. Hirsch, S. D. Peyerimhoff, and R. J. Buenker, Mol. Phys. **42**, 875 (1981).
[47] W. Meyer and P. Rosmus, J. Chem. Phys. **63**, 2356 (1975).
[48] X. Tan, Diatomic: A spectral simulation program for diatomic molecules on Windows platforms, Version 1.02, 2002, http://cs.jhu.edu/~xftan/diatomic.html
[49] K. K. Baeck and Y. S. Lee, J. Chem. Phys. **100**, 2888 (1994).
[50] C. T. Wickham-Jones, K. M. Ervin, G. B. Ellison, and W. C. Lineberger, J. Chem. Phys. **91**, 2762 (1989).
[51] Y. Chen, Q. Zhang, D. Zhang, C. Chen, S. Yu, and X. Ma, Chem. Phys. Lett. **223**, 104 (1994).
[52] M. Kakimot and E. Hirota, J. Mol. Spectrosc. **124**, 66 (1987).
[53] R. N. Dixon, G. Duxbury, and D. A. Ramsay, Proc. R. Soc. London, Ser. A **296**, 137 (1967).
[54] P. Abraham, A. Bekkaoui, J. Bouix, and Y. Monteil, J. Raman Spectrosc. **23**, 379 (1992).
[55] M. E. Jacox, in *NIST Chemistry WebBook, NIST Standard Reference Database Number 69*, edited by W. G. Mallard and P. J. Linstrom (National Institute of Standards and Technology, Gaithersburg, MD, 2003) (http://webbook.nist.gov/chemistry/).
[56] J. T. Snodgrass, J. V. Coe, C. B. Friedhoff, K. M. McHugh, and K. H. Bowen, Chem. Phys. Lett. **122**, 352 (1985).
[57] R. O. Jones, G. Ganteför, S. Hunsicker, and P. Pieperhoff, J. Chem. Phys. **103**, 9549 (1995).
[58] J. Berkowitz, L. A. Curtiss, S. T. Gibson, J. P. Greene, G. L. Hillhouse, and J. A. Pople, J. Chem. Phys. **84**, 375 (1986).
[59] J. Berkowitz (personal communication).
[60] J. Berkowitz, Acc. Chem. Res. **22**, 413 (1989).
[61] J. Berkowitz and H. Cho, J. Chem. Phys. **90**, 1 (1989).

[62]J. Berkowitz and B. Ruscic, in *Vacuum Ultraviolet Photoionization and Photodissociation of Molecules and Clusters*, edited by C. Y. Ng (World Scientific, Singapore, 1991), p. 1.
[63]M. W. Chase, Jr., *NIST-JANAF Thermochemical Tables (Journal of Physical and Chemical Reference Data, Monograph No. 9)*, 4th ed. (AIP, New York, 1998).
[64]J. E. Bartmess, J. A. Scott, and R. T. McIver, Jr., J. Am. Chem. Soc. **101**, 6046 (1979).
[65]J. E. Bartmess, in *NIST Chemistry WebBook, NIST Standard Reference Database Number 69*, edited by W. G. Mallard and P. J. Linstrom (National Institute of Standards and Technology, Gaithersburg, MD, 2003) (http://webbook.nist.gov/chemistry/).